

Voids in the 2dF Galaxy Redshift Survey

Fiona Hoyle & Michael S. Vogeley

Department of Physics, Drexel University, 3141 Chestnut Street, Philadelphia, PA 19104

hoyle@venus.physics.drexel.edu, vogeley@drexel.edu

ABSTRACT

We present an analysis of voids in the 2dF Galaxy Redshift Survey (2dFGRS). This analysis includes identification of void regions and measurement of void statistics. The 2dFGRS is the largest completed redshift survey to date, including a total of 245,591 galaxies covering 1500 deg^2 to a median depth of $z_{\text{med}} \sim 0.11$. We use the **voidfinder** algorithm to identify a total of 289 voids in the 2dFGRS with radius larger than $10h^{-1}\text{Mpc}$. These voids have an average effective radius of $14.89 \pm 2.65h^{-1}\text{Mpc}$ in the North Galactic Pole region (NGP) and $15.61 \pm 2.84h^{-1}\text{Mpc}$ in the South Galactic Pole region (SGP). These voids are extremely underdense, with average density contrast of $\delta\rho/\rho = -0.94 \pm 0.02$. The centers of voids are even emptier, because the few galaxies within the voids typically lie close to the edges. The total volume of the universe filled by these void regions is approximately 40%. These results are very similar to results found from our analysis of the PSCz survey and the Updated Zwicky Catalog; here we detect almost a factor of 10 more voids. We measure the Void Probability Function (VPF) of the 2dFGRS for volume-limited samples with limiting absolute magnitudes, $M_{\text{lim}} - 5\log(h)$, from -16 to -21 in b_J . We measure the Underdensity Probability Function (with density contrast threshold $\delta\rho/\rho = -0.8$) for samples with limiting absolute magnitudes, $M_{\text{lim}} - 5\log(h)$, from -18 to -21 . We find that the SGP is more underdense than the NGP for all but the brightest sample under consideration. There is good agreement between the VPF's of the Center for Astrophysics Survey and the 2dFGRS. Comparison of VPF's measured for the 2dFGRS with the distribution of simulated dark-matter halos of similar number density indicates that voids in the matter distribution in ΛCDM simulations are not empty enough. However, semi-analytic models of galaxy formation that include feedback effects yield VPF's that show excellent agreement with the data.

Subject headings: cosmology: large-scale structure of the universe – cosmology: observations – galaxies: distances and redshifts – methods: statistical

1. Introduction

In any map of the Universe, there appear large regions that are avoided by galaxies. These regions may not be completely empty but, compared to the rest of the Universe, are extremely underdense. We refer to these regions as voids. The giant void in Boötes was discovered more than twenty years ago (Kirshner et al. 1981) and the existence of voids was confirmed by subsequent larger surveys at a variety of wavelengths (Davis et al. 1992; de Lapparent, Geller, & Huchra 1986; da Costa et al. 1988; Geller & Huchra 1989; Maurogordato et al. 1992; da Costa et al. 1994; see Rood 1998 and references therein for a discussion of the history of void detection and interpretation). The size of the largest voids ($D \sim 30 - 50h^{-1}\text{Mpc}$) in these earlier surveys was of the same order as the characteristic depth of the surveys, which allowed speculation that even larger such structures might be found. Deeper redshift surveys, for example, the Las Campanas Redshift Survey (Shectman et al. 1996), confirmed the ubiquity of these structures, but did not detect larger voids. The recently-completed 2dFGRS (Colless et al. 2003) and the ongoing Sloan Digital Sky Survey (Abazajian et al. 2003) have the depth, areal coverage, and complete sampling of the galaxy distribution necessary to more precisely quantify the distribution of voids.

The observed spatial distribution of voids and the properties of the few galaxies that lie within them (Rojas et al. 2003a, b) can strongly constrain models for cosmology and galaxy formation. Peebles (2001) discusses an apparent discrepancy between the cold dark matter model and observations. In CDM, voids should be filled with dwarf halos with escape velocities just larger than the 20km s^{-1} or so needed to bind photoionized baryons (Dekel & Silk 1986; Hoffman, Silk, & Wyse 1992). However, surveys of dwarf galaxies indicate that they trace the same structure as that of other galaxies (Binggelli 1989). Pointed observations toward voids also fail to find a significant population of faint galaxies (Lindner et al. 1996; Kuhn, Hopp, & Elsässer 1997; Popescu, Hopp, & Elsässer 1997). This is consistent with the widely-observed result that galaxies have common voids, regardless of Hubble type (e.g., Thuan et al. 1987; Babul & Postman 1990; Mo, McGaugh, & Bothun 1994). The failure of CDM models to accurately predict the paucity of dwarfs in voids is connected to the overprediction of small satellites that would be observed in Milky-Way sized halos (Kauffmann et al. 1993; Klypin et al. 1999; Moore et al. 1999). The luminosity function of void galaxies indicates that voids are not filled with a dense population of void galaxies (Hoyle et al. 2003). Semi-analytic modeling of galaxy formation, including feedback effects, predict that galaxies in voids should be somewhat fainter, bluer, and more disk-like than galaxies in denser environments (Benson et al. 2003). Testing these predictions requires identification of large samples of void galaxies, which in turn requires detection of many large voids.

To test cosmological models, two complementary approaches may be used to describe the distribution of voids: detection of voids, i.e., treating them as individual structures and studying their properties, and characterization of large-scale structure using a variety of void statistics. A number of techniques have been developed for detecting voids, including Kauffmann & Fairall (1991), Kauffmann & Melott (1992), Ryden (1995), Ryden & Melott (1996), El-Ad & Piran (1997, EP97), and Aikio & Mähönen (1998). These algorithms have been applied to a number of galaxy surveys (Slezak, de Lapparent & Bijaoui 1993; Pellegrini, da Costa & de Carvalho 1989; El-Ad, Piran & da Costa 1996; El-Ad, Piran and da Costa 1997; Müller et al. 2000; Plionis & Basilakos 2002; Hoyle & Vogeley 2002, HV02 hereafter). The numbers of voids in each sample varies, depending on the definition of a void, but the void samples in these studies each contained fewer than 10^2 voids. In this paper we describe detection of more than 200 voids in the 2dFGRS.

The distribution of voids may also be characterized using statistics such as the Void Probability Function (VPF, White 1979) and the Underdensity Probability Function (UPF, Vogeley et al. 1989), which depend on the hierarchy of n -point correlation functions. The VPF is simply the probability that a randomly selected volume contains no galaxies. The UPF measures the frequency of regions with density contrast $\delta\rho/\rho$ below a threshold. These statistics reveal statistical information about the void population but do not give details on specific voids. Halo-occupation models of galaxy formation (e.g., Berlind & Weinberg 2002) show that statistics of voids can strongly constrain models for galaxy biasing models. Previous work on the VPF includes examination of the sky-projected galaxy distribution (Sharp 1981; Bouchet & Lachièze-Rey 1986), galaxy redshift surveys (Hamilton, Saslaw, & Thuan 1985; Maurogordato & Lachièze-Rey 1987, 1991; Fry et al. 1989; Mo & Börner 1990; Vogeley, Geller, & Huchra 1991; Lachièze-Rey, da Costa, & Maurogordato 1992; Bouchet et al. 1993; Vogeley et al. 1994), and the distribution of clusters of galaxies (Huchra et al. 1990; Jing 1990; Cappi, Maurogordato, & Lachièze-Rey 1991).

Void statistics measured for the CfA2 survey and simulations of CDM models indicate that the models can reproduce voids of bright galaxies, but fail to match the statistics of fainter galaxies (Vogeley et al. 1994; Cen & Ostriker 1998; Benson et al. 2003). These statistics show that voids in the simulations can actually appear too empty. This result strongly conflicts with the visual impression that observed voids have very smooth edges, while structures in mock redshift surveys from simulations are more diffuse (e.g., Diaferio et al. 1999). The large difference between voids in the dark matter and galaxy distributions (Ostriker et al. 2003) strongly suggests that the inconsistency lies in the details of treating galaxy formation in voids. Results of high-resolution hydrodynamic/ N -body simulations show strong density dependence of the efficiency of galaxy formation (Blanton et al. 1999; Ostriker et al. 2003). Precise measurement of the frequency of voids in samples of varying

luminosity and type will yield strong tests of the details of galaxy formation models.

In this paper, we apply the `voidfinder` analysis of HV02 and the VPF and UPF to the largest completed galaxy redshift survey, the 2 degree Field Galaxy Redshift Survey. This survey contains $\sim 250,000$ galaxies over $1,500 \text{ deg}^2$. We describe the data in more detail in section 2. In section 3, we give an overview of the `voidfinder` algorithm, present the results in section 4. In section 5 we turn our attention to the VPF and UPF, give a brief outline of these algorithms and present our results on the VPF and UPF statistics. In section 6 we summarize our results and present our conclusions.

2. The 2dFGRS

The 2dFGRS is an optical spectroscopic survey of objects brighter than $b_J \sim 19.30$ selected from the APM Galaxy Survey (Maddox et al. 1990a, b). The effective median magnitude limit of the survey is 19.30, lowered from the original magnitude limit of $b_J = 19.45$ because the photometry of the input catalog and the dust extinction maps have been revised so there are small variations in the magnitude limit as a function of position over the sky (Colless et al. 2003).

The 2dFGRS survey is divided into two main regions, with additional random fields observed to improve the angular coverage for statistics such as the power spectrum. For this analysis, we do not use the random fields as we can only find voids in regions that have a wide angular range. The two areas of interest are the South Galactic Pole (SGP) region, which covers the region $325^\circ < \alpha < 52.5^\circ$, $-37.5^\circ < \delta < -22.5^\circ$ and a region which lies toward (but not terribly close to) the North Galactic Pole (NGP), $147.5^\circ < \alpha < 222.5^\circ$, $-7.5^\circ < \delta < 2.5^\circ$. The data that we analyze are from the public release that was distributed to the community in July 2003 (Colless et al. 2003 and references therein). 245,591 galaxy redshifts were contained in the data release, making this the largest completed redshift survey to date.

The completeness of the survey varies with position on the sky because of unobserved fields (mostly around the survey edges), observed objects with poor spectra, and objects that could not be observed due to either fiber collision constraints or broken fibers. To match the angular selection function in the construction of the random catalogs, required in our void finding algorithm, we use the software developed by the 2dFGRS team and distributed as part of the data release ¹. For any given coordinates (α, δ) , the expected probability of a

¹for the data release products and catalogs see www.mso.anu.edu.au/2dFGRS

galaxy being contained in the 2dFGRS survey region is returned.

We construct volume-limited sample from the 2dFGRS to obtain a uniform radial selection function, thus the only variation in the space density of galaxies with radial distance is due to clustering. This means the chance of finding a void at any given distance in such a sample should depend only on the local clustering rather than on the changing selection function. We adopt the global k -correction + evolution correction found for b_J selected galaxies in the ESO Slice Project (Zucca et al. 1997) and adopted by the 2dFGRS team (Norberg et al. 2001) and use

$$k + e = \frac{0.03z}{(0.01 + z^4)}. \quad (1)$$

For voidfinding, we select a volume limit of $z_{\text{max}}=0.138$. This value maintains the maximum number of galaxies in the sample: 27,573 galaxies in the NGP region and 33,581 galaxies in the SGP region. We adopt a $\Omega_m = 0.3, \Omega_\Lambda = 0.7$ cosmology when converting redshift into comoving distances. For this cosmology, a redshift limit of $z_{\text{max}}=0.138$ corresponds to a comoving distance of $398h^{-1}\text{Mpc}$. For measuring void statistics, we examine sub-samples with a range of absolute-magnitude limits.

3. The Void Finding Algorithm

3.1. Outline

The void finding algorithm we adopt is described in full detail in HV02, including justification of each parameter value. The method is similar to that of EP97. The steps of the void finding algorithm are as follows:

- Classification of galaxies as wall or void galaxies
- Detecting empty cells in the distribution of wall galaxies
- Growth of the maximal empty spheres
- Classification of the unique voids
- Enhancement of the void volume

Following HV03, we calculate the mean distance, d , to the 3rd nearest galaxy. Any galaxy that has less than three neighbors in a sphere of radius $l_3 = 5.6h^{-1}\text{Mpc}$ is considered a void galaxy. The remaining galaxies are labeled as wall galaxies. We note that the value of l_3 is similar to the value used in Rojas et al. (2003a) to identify void galaxies in the SDSS.

The next step is to place the wall galaxies onto a three dimensional grid. Each empty grid cell is considered to be part of a possible void. Our method finds the maximal sphere (hole) that can be drawn in the void starting from the empty cell. We insist that the holes lie completely in the survey. At this stage we keep track of all the holes with radii larger than the value of the search radius used to classify void and wall galaxies, l_3 . The fineness of the grid defines the minimum size void that can be detected. All holes with size larger than $r = \sqrt{3}l_{\text{cell}}$, where l_{cell} is the size of each grid cell, will be detected. We use a cubical mesh that has 128 grid cells on a side, each of which is $4.7h^{-1}\text{Mpc}$ in length, thus we find all holes larger than $8.1h^{-1}\text{Mpc}$.

Finding the holes is a robust process. Deciding which of those holes are unique voids requires more thought. First we sort the holes by radius, the largest first. The largest hole found is automatically a void. We examine whether the second largest hole overlaps the void or not. If it overlaps by more than 10% in volume we say this hole is part of the first void, if not then it forms a new void. We continue like this for all holes with radii larger than $10h^{-1}\text{Mpc}$. However, if a hole overlaps more than one previously detected void by more than 10%, the hole is ignored as it links together two larger, previously identified voids.

We next enhance the volume of each void. Any hole that overlaps the maximal void sphere by 50% of the smaller hole’s volume is considered part of the larger void. If the hole overlaps with more than one void then it is not added to either of the voids as this again would link two voids together that we wish to keep separate. If the hole is isolated and less than $10h^{-1}\text{Mpc}$ in radius, it cannot be classified as a separate void as we only call a hole a void if it is larger than $10h^{-1}\text{Mpc}$ in radius.

Finally we count the number of galaxies that lie within each void to determine the underdensity of the void. Measured properties of each void include the coordinates of its center, the maximal sphere radius, the effective radius, and the average underdensity.

4. Properties of Voids

We apply the **voidfinder** algorithm to volume-limited samples of the 2dFGRS and find 116 voids in the NGP region and 173 voids in the SGP region. The properties of all the voids are available upon request and are summarized in Table 1. Figure 1 shows an example of the distribution of wall galaxies and the centers of voids in thin (1°) slices of the NGP and SGP. The filled circles show the location of the wall galaxies, the open triangles mark the centers of the voids. The SGP region covers an area that is approximately 33% larger than the NGP but it contains $\sim 50\%$ more voids. In this section we examine these voids in

detail and compare the results for the NGP and SGP regions.

4.1. Significance of the Voids

To assess the statistical significance of the detected voids, we generate 10 Poisson samples of the 2dFGRS that have the same angular selection function, distant limits, and number density as the 2dFGRS but contain no clustering. The statistical significance of a void may be estimated from (El-Ad, Piran & da Costa 1997)

$$p(r) = 1 - \frac{N_{\text{Poisson}}(r)}{N_{\text{Survey}}(r)} \quad (2)$$

where $N_{\text{Poisson}}(r)$ and $N_{\text{Survey}}(r)$ are the numbers of voids detected by applying `voidfinder` to random samples and galaxy samples, respectively. In Figure 2, we show the number of voids with radius greater than r that we find in the NGP and SGP added together (triangles) as compared to the random catalogs (squares). In the same plot, we present the significance of the voids. Voids larger than $10h^{-1}\text{Mpc}$ are significant at the $> 90\%$ level, consistent with results in HV02. The statistical significance of voids rapidly approaches 100% as the void radii increase; the false positive rate for voids with average radius $r \sim 12h^{-1}\text{Mpc}$ is well below 1%.

4.2. Sizes of the Voids

The mean maximal sphere size, with minimum size of $10h^{-1}\text{Mpc}$, is $12.09 \pm 1.85h^{-1}\text{Mpc}$ for the NGP and $12.52 \pm 1.99h^{-1}\text{Mpc}$ for the SGP so the two samples of voids have similar average sizes, although the voids in the SGP are slightly larger. Average values of effective radius are slightly larger, $14.89 \pm 2.65h^{-1}\text{Mpc}$ for the NGP and $15.61 \pm 2.84h^{-1}\text{Mpc}$ for the SGP. Figure 3 shows histograms of the distribution of void sizes. The distribution of the maximal spheres are shown in the left and the effective radii on the right. The NGP distribution peaks at lower radii, suggesting that the SGP region is slightly emptier. Statistical comparison of the distributions of void sizes using a Kolmogorov-Smirnov test

Region	N_{voids}	r ($h^{-1}\text{Mpc}$)	r_{eff} ($h^{-1}\text{Mpc}$)	$\delta\rho/\rho$	Volume
NGP	116	$12.09 \pm 1.85h^{-1}\text{Mpc}$	$14.89 \pm 2.65h^{-1}\text{Mpc}$	-0.94 ± 0.02	33.4%
SGP	173	$12.52 \pm 1.99h^{-1}\text{Mpc}$	$15.61 \pm 2.84h^{-1}\text{Mpc}$	-0.93 ± 0.02	41.6%

Table 1: The properties of the voids in the NGP and SGP

reveals that the NGP and SGP void size distributions are different only at the 6% level, thus the volume of these samples are just large enough to overcome variations of the large-scale structures within them (a.k.a., cosmic variance).

4.3. Density of Voids

The galaxies in the NGP and SGP samples are split into wall/void galaxies as described in section 3. Approximately 10% of galaxies lie in low density regions, are classified as void galaxies, and could reside in the void regions. However, due to the shapes of the voids, some of the void galaxies do not lie within the detected voids, but rather lie at the edges near a higher density region. In the NGP, 1518 of the 2296 void galaxies reside in a void and in the SGP, 2319 of the 3992 void galaxies are found in a void, thus 5.5% and 6.9% of the galaxies lie in voids. These results are consistent with our analysis of the UZC and PSCz (HV02) and results of El-Ad, Piran & da Costa (1997).

The 5-7% of galaxies that lie within voids inhabit extremely rarified regions of the universe. The average density contrast of voids is $\delta\rho/\rho = -0.94 \pm 0.02$ and -0.93 ± 0.02 for the NGP and SGP, respectively. If we examine the density profiles of voids in detail, we find that the centers of voids are even more empty, with density contrast approaching $\delta\rho/\rho = -1$, i.e., zero density of galaxies. To consistently compare the density profiles of voids of varying size, we normalize distances from the void center by the maximal sphere size for each voids. Thus, we measure density as a function of r/R_{max} . In other words, a galaxy lying $6h^{-1}\text{Mpc}$ from the center of a $12h^{-1}\text{Mpc}$ void is considered to be at the same ‘distance’ as a galaxy $8h^{-1}\text{Mpc}$ from the center of a $16h^{-1}\text{Mpc}$ void. The average effective radius for the voids is $\sim 15h^{-1}\text{Mpc}$. We calculate the density of the void assuming this average size and compare the average density of the two regions to calculate $\delta\rho/\rho$.

In Figure 4, we show the average density contrasts within voids in the NGP (solid line) and SGP (dashed line). The voids are extremely underdense in the centers. Even at 90% of the void radius the density contrast remains below $\delta\rho/\rho = -0.9$. The density of the void then sharply rises at the maximal sphere radius. indicative of the fact that we have accurately found the walls surrounding the voids. Even at twice the void radius, the voids still trace underdense regions. The same trend is seen in both the NGP and the SGP. The profiles of the voids show how well the void finder algorithm works in detecting empty regions. The 10% or so of galaxies that are allowed to reside in void regions tend to lie close to the edges of the voids.

Tests of `voidfinder` using cosmological simulations also show how well this algorithm

works. Using semi-analytic models applied to CDM simulations, Benson et al. (2003) created mock galaxy catalogs with the same density as the 2dFGRS and SDSS. When applied to these mock samples, **voidfinder** accurately detected the edges of voids. Comparison of the density profiles of the voids in the mock galaxies with the density profiles of dark matter showed that the sharp transition from void to wall was seen in both galaxies and dark matter.

4.4. Void Size as a Function of Redshift

The Λ CDM model with parameters inferred from the WMAP measurements of the CMB anisotropy (Bennett et al. 2003) is able to reproduce the large-scale structure of the universe. On small scales there are some problems, as the models produce too much substructure, but perhaps this problems can be addressed by including the physics of galaxy formation. On the scale of voids, this basic model for formation of structure via gravitational instability in a universe in which gravitational potential fluctuations are dominated by dark matter seems fairly secure. During the evolution of large-scale structure, voids deepen and expand in comoving size. We might, therefore, be able to detect this growth if we can examine void sizes over a sufficient range of redshift.

The volume-limited samples we extract from the 2dFGRS extend to $z_{\text{max}}=0.138$, which corresponds to a comoving distance of $\sim 400h^{-1}\text{Mpc}$. To make a first test for the variation with redshift of void size, we divide our void sample into three ranges of comoving distance and compare the histograms of void sizes. In Figure 5, we combine the voids in the NGP and SGP and compare the distributions of voids whose centers lie at $r < 200h^{-1}\text{Mpc}$ (long dashed line), $200 < r < 300h^{-1}\text{Mpc}$ (short dashed line) and $300 < r < 400h^{-1}\text{Mpc}$ (solid line). If void sizes grow with time, we would expect the nearby sample to contain larger voids. However, here we find that the most distant samples contain the largest voids. Clearly, the 2dFGRS does not extend deep enough to observe the growth of voids. To leading order, structure growth freezes out at a redshift of $\sim 1/\Omega_m$ which is around $z \sim 3$ for a $\Omega_m = 0.3$, $\Omega_\Lambda = 0.7$ cosmology, so little evolution could be detected in the samples here.

4.5. Volume of the Universe Contained in Voids

We estimate the total volume of the 2dFGRS contained in the voids using random catalogs which have the same angular and radial selection function as the volume limited catalogs but the particles are unclustered. Each random particle is tested as to whether it lies in a void region or not and the volume contained in voids is the simply the number of

random particles that lie in the voids, divided by the total number of random particles. This procedure is essentially a Monte Carlo integration over the strangely-shaped volumes of all the voids (recall that the final merged voids are not exactly spherical). We find that 33.4% of the NGP volume is contained in a void and 41.6% of the SGP region is contained in a void. This is consistent with early findings that the SGP is emptier than the NGP. Note carefully that the fraction of space filled by voids depends strongly on the definition of “void.” As shown by Figure 4, we count only the deep interior of voids, excluding the transition zone near the dense structures. Thus, these voids are structures with extremely low mean density, $\delta\rho/\rho < -0.9$.

4.6. Comparison with Voids in the UZC and PSCz

Voids have previously been detected in the Updated Zwicky Catalog and the PSCz survey using `voidfinder` (HV02) and other authors have applied different void finding methods to detect voids in other surveys (see, for example Slezak, de Lapparent & Bijaoui 1993; Pellegri, da Costa & de Carvalho 1989; El-Ad, Piran & da Costa 1996, 1997; Müller et al. 2000; Plionis & Basilakos 2001). It would be interesting to compare the void catalogs using different methods, but because of the narrow opening angle of the 2dFGRS, it is not possible to detect voids in the very local volume examined by most previous studies, thus a direct void by void comparison is ruled out. A comparison between voids found in all of these different samples was made in HV02. Here we concentrate on comparing the properties of 2dFGRS voids with those found in the UZC and PSCz samples using the same technique.

A concern in our analysis of the UZC and PSCz survey was that the edge of the survey restricted the sizes of the voids. This effect is less important in the 2dFGRS, thus comparison of the distribution of void sizes may indicate whether analyses of the shallower catalogs was biased. The average effective radius of voids in the UZC and PSCz is 14.9 ± 1.8 and $14.6 \pm 1.4 h^{-1} \text{Mpc}$, respectively. The average effective radius of voids in the 2dFGRS is $14.89 \pm 2.65 h^{-1} \text{Mpc}$ and $15.61 \pm 2.84 h^{-1} \text{Mpc}$ for the NGP and SGP regions, respectively. The void sizes are comparable, suggesting that the sizes of voids in the UZC and PSCz were not underestimated. The densities of voids are also comparable. Voids in the 2dFGRS have average density contrast $\delta\rho/\rho = -0.94 \pm 0.02$ and -0.93 ± 0.02 in the NGP and SGP, respectively. The UZC and PSCz voids have $\delta\rho/\rho = -0.92 \pm 0.03$ and -0.96 ± 0.01 . This agreement and the quite similar percentages of galaxies that are classified as void galaxies in both studies indicates that this method of identifying voids is robust with respect to variation in galaxy selection and survey geometry.

5. Void Statistics

5.1. The Void Probability and Underdensity Probability Functions

We statistically quantify the the probability of finding voids in the 2dFGRS using the Void Probability Function (VPF) (White 1979; see also Lachièze-Rey, da Costa & Maurogordato 1992; Watson & Rowan-Robinson 1993; Vogeley, Geller & Huchra 1991; Benson et al. 2003). The VPF gives the probability that a randomly selected volume of a survey contains no galaxies. In reality the region might contain galaxies that are below the magnitude limit of the survey but there are no survey galaxies in the randomly chosen region.

The VPF depends on all the n-point correlation functions according to (White 1979)

$$P_0(n, V) = \exp \left[\sum_{N=1}^{\infty} \frac{(-n)^N}{N!} \int_V w_N(\mathbf{x}_1, \dots, \mathbf{x}_N) d^3x_1 \dots d^3x_N \right] \quad (3)$$

where n is the average number density of galaxies, w_N are the n-point correlation functions and x_i are the galaxy positions in the volume V . The simplest case is a Poisson distribution where

$$P_0 = e^{-nV} \quad (4)$$

Here we examine spherically symmetric test volumes, thus $P_0 = P_0(r)$, where r is the radius of a test sphere.

A disadvantage of the VPF is its sensitivity to shot noise, because a single galaxy changes the contribution of a large void to the statistic. A related, somewhat more robust, statistic is the underdensity probability function (UPF), which measures the probability of the density lying below a selected threshold in a region of scale r ,

$$U(r) = P(\rho < \rho_{\text{crit}}; r) \quad (5)$$

which is an integral over the low- ρ tail of the density distribution function. As with the VPF, we measure the UPF for spherically symmetric regions. As discussed below, we measure the UPF for an underdensity threshold of $\delta\rho/\rho = -0.8$, just slightly denser than the mean underdensity of the large voids detected in section 4 above.

The method of calculating both the VPF ($P_0(r)$) and UPF ($U(r)$) is straightforward. A point is randomly chosen within the survey volume. The first test is to see if a sphere of radius r lies completely in the survey or not. If so, then the number of galaxies that lies in this sphere is counted. This is repeated many times for different sphere radii. The VPF is then simply estimated as $P_0 = N_0/N_{\text{test}}$ and the estimator for the UPF is $U(r) = N_{(\rho < \rho_{\text{crit}})}/N_{\text{test}}$.

The probability of finding a void increases with distance in flux limited samples due to the decreasing selection function as faint galaxies become too faint to be detected by the survey. Some earlier analyses (Vogeley, Geller & Huchra 1991; Lachièze-Rey, da Costa & Maurogordato 1992; Watson & Rowan-Robinson 1993) concentrated on measuring the VPF from flux-limited samples, to maximize use of smaller redshift samples. The sizes of voids were rescaled to compensate for the decreasing selection function. Here we follow Vogeley et al. (1994), who measured the VPF of volume-limited samples from the CfA2 survey with limiting absolute magnitudes $M_{\text{lim}} - 5\log h = -18.5, -19, -19.5$ and -20 . The VPF results from volume-limited samples are easier to interpret as there is no need to rescale the sizes of voids and one can compare results from samples with the same average number density drawn from other surveys.

5.2. VPF Results for the 2dFGRS

We measure the VPF of volume-limited samples drawn from the 2dFGRS. The details of each sample are given in Table 2. We present results for the VPF in Figures 6 and 7. In Figure 6 we show the VPF from various volume limited samples extracted from the NGP (left hand plot) and SGP (right hand plot). For clarity, error bars are shown on the $M_{\text{lim}} - 5\log h = -19$ and -21 samples. These uncertainties are the 1σ variation due to the finite number of independent volumes in the 2dFGRS. The binomial distribution of void counts yields the uncertainty estimate

$$\sigma(P_0) = \frac{(P_0 - P_0^2)^{1/2}}{N_{\text{indep}}^{1/2}} \quad (6)$$

where $N_{\text{indep}} = V_{\text{survey}}/(4\pi r_{\text{test}}^3/3)$. As expected, the void probabilities are larger in samples of brighter galaxies because the average number density is smaller. We estimate the VPF for 6 volume-limited samples with limiting absolute magnitudes $M_{\text{lim}} - 5\log h$ from -16 to -21 . The values of the VPF are available in Tables 3 and 4. This study of void statistics probes the widest range of galaxy luminosities to date.

We compare the VPF of the NGP (solid lines) and SGP (dashed lines) of 4 of the 6 samples in Figure 7. Only the samples with $M_{\text{lim}} - 5\log h = -17, -19, -20$ and -21 ($z_{\text{max}}=0.039, 0.126, 0.182$ and 0.270) are shown for clarity. We see that locally, i.e. in the fainter sub-samples, there is a higher probability of finding voids in the SGP than in the the NGP (the lines are shifted to the right). This result is consistent with the result discussed above using `voidfinder`, which shows that the SGP is somewhat emptier than the NGP. In the brightest sample, however, we find that voids are more likely to be detected in the NGP.

We attribute these variations to large-scale inhomogeneity on the scales of these samples. It can be seen in Table 2 that in the all but the brightest samples, the SGP has a lower number density of galaxies than the NGP, thus a higher probability of detecting voids would be expected. In the $M_{\text{lim}} - 5\log h = -21$ samples, the NGP has a slightly lower number density than the SGP and the chance of finding voids is larger.

We use mock catalogs from the Hubble Volume (Evrard et al. 2002) simulation to assess the different ways in which errors of the VPF can be estimated. In Figure 8, we compare the errors found using equation 6 (triangles), which are referred to as Poisson errors as they depend on the number of independent volumes in the survey area, and the dispersion over 10 mock catalogs (circles). We show the results for the NGP (filled symbols) and SGP (open symbols). The errors follow the same trend and are in reasonable agreement. On small scales, the Poisson errors underestimate the error from the mocks, whereas on large scales, the Poisson errors overestimate the errors from the mock catalogs, as the number of independent volumes decreases as the size of the void grows.

5.3. Underdensity Probabilities of the 2dFGRS

In Figure 9 we present results of the UPF estimated for the same volume-limited samples of the NGP and SGP regions. For this analysis, we choose an underdensity threshold of $\delta\rho/\rho = -0.8$, which is slightly less restrictive than the density contrast $\delta\rho/\rho < -0.9$ of the voids found in section 4. If we were to choose a more extreme density threshold, the UPF would be almost equivalent to the VPF because voids are discrete objects. As estimated here, the UPF probes the regions near the boundary between the voids and denser structures.

In Figure 9 we plot the UPF for a threshold $\delta\rho/\rho = -0.8$ for volume-limited samples with $M_{\text{lim}} - 5\log h = -18, -19, -20$ and -21 and the data are available in Tables 5 and

$M_{\text{lim}} - 5\log h$	z_{max}	N_{gal} NGP	N_{gal} SGP	\bar{n} NGP $h^{-3}\text{Mpc}^3$	\bar{n} SGP $h^{-3}\text{Mpc}^3$
-16	0.039	4076	4928	0.0560	0.0477
-17	0.058	8686	9345	0.0360	0.0273
-18	0.087	21128	21752	0.0282	0.0200
-19	0.126	27162	33667	0.0114	0.0099
-20	0.182	19151	25139	0.0028	0.0010
-21	0.270	4123	7084	0.00019	0.00023

Table 2: The properties of the volume limited samples used in the VPF and UPF calculations.

6. As for the VPF, the chance of finding an underdense region increases as the magnitude limit of the samples brightens and the number density of objects in the sample decreases.

In Figure 10, we compare the UPF’s for three volume-limited samples with $M_{\text{lim}} - 5\log h = -19, -20$ and -21 of both the NGP and SGP regions. Again, we find that the SGP is more underdense than the NGP, but in this case we find good agreement in the brightest samples.

5.4. Comparison With Previous Work

The VPF and UPF have previously been estimated from the Center for Astrophysics survey (de Lapparent et al. 1986; Geller & Huchra 1989; Huchra et al. 1999) by Vogeley et al. (1994). In Figure 11, we compare the measurements of the VPF of the CfA survey to those from the 2dFGRS. To get an overall measurement for the 2dFGRS for each magnitude cut, we average the VPF’s of the NGP and SGP, weighted by their respective errors. Uncertainties on the VPF’s of the 2dFGRS samples are significantly smaller than those for the CfA due to the larger volume of the 2dFGRS.

Comparison of these results is complicated by the possibility, suggested by comparison with CCD photometry, that the Zwicky magnitude system is not simply offset in zeropoint from b_J , but also suffers a significant scale error (Gaztañaga & Dalton 2000). Here we make the simplest assumption – assuming an offset of $m_Z = b_J + 0.5$ (as suggested by Efstathiou et al. 1988 and Lin et al. 1994) – that we can compare the VPF’s of the $M_{\text{lim}} - 5\log h = -19.0$ 2dFGRS sample and -18.5 CfA2 sample. These VPF’s agree within the quite large uncertainties of the CfA2 sample. The VPF of the latter is systematically smaller, but note carefully that values of P_0 at different r are not independent. Although there is better agreement if we compare the -19.0 samples, it seems more likely that the smaller volume of CfA2 causes the VPF to be low than that the magnitude systems match. Likewise, we may compare the -20.0 2dFGRS sample with the -19.5 CfA2 sample. Again, these agree within the large uncertainties and again we suspect that a combination of cosmic variance and problems with comparing the magnitude systems causes the offset.

5.5. Comparison with VPF’s in Simulations

In Figure 12, we compare the VPF’s of the data with the VPF of mock catalogs drawn from a dark matter only Λ CDM simulation, the *Hubble Volume* (Evrard et al. 2002). The dark matter only mock catalogs contain too much substructure on small scales and fail to

match the VPF’s of the data, as seen in Benson et al. (2003).

A better comparison between theory and data can be made by using mock galaxy catalogs constructed using semi-analytic models of galaxy formation, as done by Benson et al. (2003), who measure the VPF of mock 2dFGRS samples. In Figure 13, we show the VPF’s from the models (symbols) and 2dFGRS data (lines). The models have $M_{\text{lim}} - 5\log h = -18.7$ and -20 , close to the limits of -19 and -20 for our observed 2dFGRS samples. The agreement between the data and theory is excellent. This agreement, in contrast to the strong disagreement with the VPF of random samples of the dark matter distribution, shows the importance of including more detailed physics in the prescription for forming galaxies in simulations. We look forward to comparisons of these measurements of void statistics with results from high-resolution cosmological hydrodynamic/N-body simulations.

6. Summary and Conclusions

We quantify the distribution of voids in the 2dFGRS by applying an objective void-finding algorithm (**voidfinder**) and by measuring the frequency of empty and underdense regions. These statistics provide strong constraints on models for structure formation.

Results of this work include a new catalog of 289 voids: 116 in the NGP region and 173 in the SGP region. This sample is almost a factor of 10 larger than previously identified. The larger number of voids in the SGP reflects both its larger volume and slightly lower average density of galaxies. These voids have minimum radii of $10h^{-1}\text{Mpc}$, an average effective radius of $15h^{-1}\text{Mpc}$, and average density contrast $\delta\rho/\rho = -0.94$.

Examination of the density profile of the voids shows that the **voidfinder** algorithm identifies the inner region of the voids where the galaxy density is nearly constant, varying from $\delta\rho/\rho \sim -0.9$ at the outer edge and decreasing toward zero density near the center. Just outside the boundary of the voids, the galaxy density sharply rises, although the mean density remains well below $\delta\rho/\rho = -0.5$ out to 150% of the void radius.

These extremely underdense voids fill 40% of the volume of the survey. The voids contain 5% of all galaxies in the sample. All of the measured properties of voids found in the 2dFGRS agree with void properties of the more nearby galaxy distributions sampled by the UZC and PSCz survey (HV02), indicating that this algorithm for identifying voids is robust with respect to variation in galaxy selection and survey geometry. Comparable results are found using a similar algorithm applied to the IRAS 1.2Jy (El-Ad, Piran, & da Costa 1997), SSRS2 (El-Ad & Piran 1997), and ORS (El-Ad & Piran 2000).

We measure the Void Probability Function and Underdensity Probability Function of volume-limited samples. These statistics quantify the frequency of completely empty and underdense spheres, respectively. We present the VPF's and UPF's for the widest range of absolute magnitudes examined to date: from -16 to -21 for the VPF and -18 to -21 for the UPF. Variation of these statistics between the two survey regions reflect underdensity of the SGP relative to the NGP out to comoving distance $400h^{-1}\text{Mpc}$. We find reasonable agreement between the VPF's of the 2dFGRS and results from the largest previous study, of the CfA2 survey (Vogeley et al. 1994). The larger volume of the 2dFGRS makes these new VPF measurements significantly more precise than could be estimated from CfA2.

Comparison of void statistics of 2dFGRS with results for the distribution of dark matter particles in large cosmological N-body simulations show that the matter distribution of the models does not have the correct VPF. However, application of semi-analytic modeling to results of high-resolution dark matter simulations (Benson et al. 2003) yields mock galaxy catalogs that provide uncanny agreement with the VPF measured for the 2dFGRS.

Void statistics will yield more precise constraints on structure formation models as we examine samples that cover even larger volume and include more information about intrinsic properties of the galaxies. The larger volume, five-band photometry, and medium-resolution spectroscopy of the Sloan Digital Sky Survey will allow precise measurement of void statistics, even after subdividing samples by galaxy property. On the theoretical side, improvement in the dynamic range of cosmological simulations and the inclusion of more sophisticated treatment of hydrodynamics and energy feedback will yield more realistic modeling of the formation of the few galaxies that lie in cosmic voids.

MSV acknowledges support from NSF grant AST-0071201. We acknowledge the enormous efforts of all involved with the 2dF project and thank them for providing this wonderful data set.

REFERENCES

- Abazajian, K., et al., 2003, AJ, 126, 208
- Aikio, J., & Mähönen, P. 1998, ApJ, 497, 534
- Babul, A., & Postman, M., 1990, ApJ, 359, 280
- Berlind, A., & Weinberg, D.H. 2002, ApJ, 575, 587
- Bennett, C. L., et al., 2003, ApJS, 148, 1

- Benson, A. J., Hoyle, F., Torres, F & Vogeley, M. S., 2003, MNRAS, 340, 160
- Bingelli, B., 1989, in Large-Scale Structure and Motions in the Universe, ed. M. Mezetti, Dordrecht: Kluwer, 47
- Blanton, M., Cen, R., Ostriker, J. P. & Strauss, M. A., 1999, ApJ, 522, 590
- Bouchet, F. R. & Lachièze-Rey, M., 1986, ApJ, 302, 37
- Bouchet, F. R., Strauss, M. A., Davis, M., Fisher, K. B., Yahil, A. & Huchra, J. P., 1993, ApJ, 417, 36
- Capri, A., Maurogordato, S. & Lachièze-Rey, M., 1991, A&A, 243, 28
- Cen, R. & Ostriker, J. P. 1998, ApJ, 514, 1
- Colless, M., et al., 2003, MNRAS, astro-ph/0306581
- da Costa, L.N., et al., 1988, ApJ, 327, 544
- da Costa, L.N., et al., 1994, ApJ, 424
- Davis, M., Huchra, J.P., Latham, D.W., & Tonry, J., 1992, ApJ, 253, 423
- Dekel, A., & Silk, J. 1986, ApJ, 303, 39
- de Lapparent, V., Geller, M.J., & Huchra, J.P., 1986, ApJ, 302, L1
- Diaferio, A., Kauffmann, G., Colber, J. M. & White, S. D. M., 1999, MNRAS, 307, 537
- Efstathiou G., Ellis, R., & Peterson, B.J. 1988, MNRAS, 232, 431
- El-Ad, H., & Piran, T. 1997, ApJ, 491, 421
- El-Ad, H., & Piran, T. 2000, MNRAS, 313, 553
- El-Ad, H., Piran, T., & da Costa, L.N. 1996, ApJ, 462, 13
- El-Ad H., Piran, T., & da Costa, L.N. 1997, MNRAS, 287, 790
- Evrard, A. E. et al., 2002, ApJ, 573, 7
- Fry, J. N., Giovanelli, R., Haynes, M. P., Melott, A. L. & Scherrer, R. J., 1989, ApJ. 340, 11
- Gaztañaga, E., & Dalton, G.B. 2000, MNRAS, 312, 417
- Geller, M. J., & Huchra, J. P., 1989, Science, 246, 857

- Hamilton, A. J. S., Saslaw, W. C. & Thuan, T. X., 1985, *ApJ* 297, 37
- Hoffman, Y., Silk, J., & Wyse, R.F.G. 1992, *ApJ*, 388, L13
- Hoyle, F. & Vogeley, M. S., 2002, *ApJ*, 566, 641
- Hoyle, F., Rojas, R., Vogeley, M.S., & Brinkmann, J. 2003, *ApJ*, submitted, astro-ph/0309728
- Huchra, J.P., Geller, M. J., Henry, J. P. & Postman, M., 1990, *ApJ*, 365, 66
- Huchra, J. P., Vogeley, M. S., & Geller, M. J., 1999, *ApJS*, 121, 287
- Jing, Y. P., 1990, *A&A*, 233, 309
- Kauffmann, G., & Fairall, A.P., 1991, *MNRAS*, 248, 313
- Kauffmann, G., & Melott, A.L. 1992, *ApJ*, 393, 415
- Kauffmann, G., White, S. D. M. & Guiderdoni, B., 1993, *MNRAS*, 264, 201
- Kirshner, R.P., Oemler, A. Jr., Schechter, P.L., & Shectman, S.A. 1981, *ApJ*, 248, L57
- Klypin, A., Kravtsov, A. V., Valenzuela, O. & Prada, F., 1999, *ApJ*, 522, 82
- Kuhn, B., Hopp, U., & Elaässer, H., 1997, *A&A*, 318, 405
- Lachière-Rey, M., da Costa, L. N. & Maurogordato, S., 1992, *ApJ*, 399, 10
- Lin, H. et al. 1994, *ApJ*, 464, 60
- Lindner, U. et al., 1996, *A&A*, 314, 1
- Maddox, S. J., Efstathiou, G., Sutherland, W. J. & Loveday, J., 1990a, *MNRAS*, 243, 692
- Maddox, S. J., Efstathiou, G. & Sutherland, W. J., 1990b, *MNRAS*, 246, 433
- Maurogordato, S. & Lachière-Rey, M., 1987, *ApJ*, 320, 13
- Maurogordato, S. & Lachière-Rey, M., 1991, *ApJ*, 369, 30
- Maurogordato, S., Schaeffer, R. & da Costa, L.N., 1992, *ApJ*, 390, 17
- Marzke, R. O., Huchra, J. P & Geller, M. J. 1994, *ApJ*, 428, 43
- Mo, H. J. & Börner, G., 1990, *A&A*, 238, 3

- Mo, H.J., McGaugh, S.S., & Bothun, G.D., 1994, MNRAS, 267, 129
- Moore, B., Ghigna, S., Governato, F., Lake, G., Quinn, T., Stadel, J., & Tozzi, P., 1999, ApJ, 524, 19
- Müller, V., Arabi-Bidgoli, S., Einasto, J., & Tucker, D. 2000, MNRAS, 318, 280
- Norberg, P. et al., 2001, MNRAS, 328, 64
- Norberg, P. et al., 2002, MNRAS, 336, 907
- Ostriker, J. P., Nagamine, K., Cen, R. & Fukugita, M., 2003, ApJ, 597, 10
- Peebles, P.J.E., 2001, ApJ, 557, 495
- Pellegrini, P.S., da Costa, L.N., & de Carvalho, R.R., 1989, 339, 595
- Plionis, M., & Basilakos, S. 2002, MNRAS, 330, 399
- Popescu, C., Hopp, U., & Elaässer, H., 1997, A&A, 325, 881
- Rojas, R., Vogeley, M. S., Hoyle, F. & Brinkmann, J., 2003a, ApJ submitted, astro-ph/0307274
- Rojas, R., Vogeley, M. S., Hoyle, F. & Brinkmann, J., 2003b, in preparation
- Rood, H.J., 1988, ARA&A, 26, 245
- Ryden, B.S. 1995, ApJ, 452, 25
- Ryden, B.S., & Melott, A.L. 1996, ApJ, 470, 160
- Sharp, N.A., 1981, MNRAS, 195, 857
- Shectman, S., A., Landy, S., D., Oemler, A., Tucker, D., L., Lin, H., Kirshner, R., P. & Schechter, P., L., 1996, ApJ, 470, 172
- Slezak, E., de Lapparent, V., & Bijaoui, A., 1993, ApJ, 409, 517
- Thuan, T.X., Gott, J.R. III, & Schneider, S.E., 1987, ApJ, 315, L93
- Vogeley, M.S., Geller, M.J., & Huchra, J.P., 1989, BAAS, 21, 1171
- Vogeley, M.S., Geller, M.J., & Huchra, J.P., 1991, ApJ, 382, 44
- Vogeley, M.S., Geller, M.J., Park, C., & Huchra, J.P., 1994, ApJ, 108, 745

Watson, J. M. & Rowan-Robinson, M., 1993, MNRAS, 265, 1027

White, S.D.M., 1979, MNRAS, 189, 831

Zucca, E., et al., 1997, A&A, 326, 477

r ($h^{-1}\text{Mpc}$)	-17	-18	-19	-20	-21
1	0.9200±0.0011	0.9410±0.0005	0.9680±0.0002	0.9920±0.0001	0.9990±0.0000
2	0.6740±0.0055	0.7280±0.0029	0.8280±0.0014	0.9390±0.0005	0.9960±0.0001
3	0.4340±0.0107	0.4820±0.0059	0.6190±0.0033	0.8320±0.0015	0.9830±0.0003
4	0.2570±0.0146	0.2760±0.0082	0.4180±0.0052	0.6880±0.0029	0.9580±0.0007
5	0.1280±0.0156	0.1290±0.0086	0.2480±0.0064	0.5260±0.0043	0.9250±0.0013
6	0.0564±0.0141	0.0559±0.0077	0.1280±0.0065	0.3690±0.0055	0.8740±0.0022
7	0.0243±0.0119	0.0131±0.0048	0.0606±0.0059	0.2500±0.0062	0.8100±0.0032
8	0.0020±0.0042	0.0040±0.0033	0.0265±0.0048	0.1500±0.0063	0.7350±0.0044
9	0.0000±0.0000	0.0013±0.0022	0.0080±0.0032	0.0781±0.0056	0.6550±0.0057
10	0.0000±0.0000	0.0001±0.0007	0.0012±0.0015	0.0435±0.0050	0.5730±0.0069
11	0.0000±0.0000	0.0000±0.0000	0.0001±0.0005	0.0183±0.0038	0.5010±0.0081
12	0.0000±0.0000	0.0000±0.0000	0.0000±0.0000	0.0058±0.0025	0.4170±0.0091
13	0.0000±0.0000	0.0000±0.0000	0.0000±0.0000	0.0027±0.0019	0.3300±0.0098
14	0.0000±0.0000	0.0000±0.0000	0.0000±0.0000	0.0003±0.0007	0.2830±0.0105
15	0.0000±0.0000	0.0000±0.0000	0.0000±0.0000	0.0000±0.0000	0.2140±0.0106
16	0.0000±0.0000	0.0000±0.0000	0.0000±0.0000	0.0000±0.0000	0.1670±0.0106
17	0.0000±0.0000	0.0000±0.0000	0.0000±0.0000	0.0000±0.0000	0.1260±0.0103
18	0.0000±0.0000	0.0000±0.0000	0.0000±0.0000	0.0000±0.0000	0.0979±0.0101
19	0.0000±0.0000	0.0000±0.0000	0.0000±0.0000	0.0000±0.0000	0.0694±0.0093
20	0.0000±0.0000	0.0000±0.0000	0.0000±0.0000	0.0000±0.0000	0.0469±0.0084
21	0.0000±0.0000	0.0000±0.0000	0.0000±0.0000	0.0000±0.0000	0.0325±0.0076
22	0.0000±0.0000	0.0000±0.0000	0.0000±0.0000	0.0000±0.0000	0.0230±0.0069

Table 3: Void Probability Function $P_0(r)$ measured measured for volume-limited samples of the NGP region with absolute magnitude limits $M_{\text{lim}} - 5\log h = -17, -18, -19, -20$ and -21 .

r ($h^{-1}\text{Mpc}$)	-17	-18	-19	-20	-21
1	0.9350±0.0009	0.9500±0.0004	0.9730±0.0002	0.9920±0.0001	0.9990±0.0000
2	0.7200±0.0044	0.7650±0.0023	0.8580±0.0011	0.9450±0.0004	0.9950±0.0001
3	0.4590±0.0091	0.5370±0.0050	0.6680±0.0027	0.8630±0.0012	0.9800±0.0003
4	0.2650±0.0124	0.3330±0.0072	0.4780±0.0044	0.7330±0.0023	0.9560±0.0006
5	0.1170±0.0126	0.1830±0.0083	0.2970±0.0057	0.5830±0.0036	0.9220±0.0011
6	0.0443±0.0106	0.0807±0.0077	0.1740±0.0062	0.4320±0.0047	0.8710±0.0018
7	0.0167±0.0083	0.0358±0.0066	0.0843±0.0057	0.3060±0.0056	0.7990±0.0028
8	0.0039±0.0049	0.0145±0.0052	0.0427±0.0051	0.1980±0.0059	0.7340±0.0037
9	0.0005±0.0021	0.0052±0.0037	0.0161±0.0038	0.1240±0.0058	0.6440±0.0048
10	0.0000±0.0000	0.0018±0.0026	0.0069±0.0029	0.0714±0.0053	0.5500±0.0059
11	0.0000±0.0000	0.0000±0.0000	0.0019±0.0018	0.0345±0.0043	0.4640±0.0068
12	0.0000±0.0000	0.0000±0.0000	0.0001±0.0005	0.0156±0.0034	0.3750±0.0075
13	0.0000±0.0000	0.0000±0.0000	0.0000±0.0000	0.0066±0.0025	0.2930±0.0079
14	0.0000±0.0000	0.0000±0.0000	0.0000±0.0000	0.0026±0.0017	0.2230±0.0081
15	0.0000±0.0000	0.0000±0.0000	0.0000±0.0000	0.0013±0.0014	0.1670±0.0081
16	0.0000±0.0000	0.0000±0.0000	0.0000±0.0000	0.0000±0.0000	0.1180±0.0077
17	0.0000±0.0000	0.0000±0.0000	0.0000±0.0000	0.0000±0.0000	0.0800±0.0071
18	0.0000±0.0000	0.0000±0.0000	0.0000±0.0000	0.0000±0.0000	0.0534±0.0064
19	0.0000±0.0000	0.0000±0.0000	0.0000±0.0000	0.0000±0.0000	0.0311±0.0054
20	0.0000±0.0000	0.0000±0.0000	0.0000±0.0000	0.0000±0.0000	0.0174±0.0044
21	0.0000±0.0000	0.0000±0.0000	0.0000±0.0000	0.0000±0.0000	0.0092±0.0034
22	0.0000±0.0000	0.0000±0.0000	0.0000±0.0000	0.0000±0.0000	0.0048±0.0027

Table 4: Void Probability Function $P_0(r)$ measured for volume-limited samples of the SGP region with absolute magnitude limits $M_{\text{lim}} - 5\log h = -17, -18, -19, -20$ and -21 .

$r \ (h^{-1}\text{Mpc})$	-18	-19	-20	-21
1	0.9410±0.0005	0.9680±0.0002	0.9920±0.0001	0.9990±0.0000
2	0.7290±0.0029	0.8280±0.0014	0.9390±0.0005	0.9960±0.0001
3	0.4820±0.0059	0.6190±0.0033	0.8320±0.0015	0.9830±0.0003
4	0.2760±0.0082	0.4180±0.0052	0.6880±0.0029	0.9580±0.0007
5	0.2200±0.0106	0.2480±0.0064	0.5260±0.0043	0.9250±0.0013
6	0.1880±0.0131	0.2230±0.0081	0.3690±0.0055	0.8740±0.0022
7	0.1170±0.0136	0.1750±0.0093	0.2500±0.0062	0.8100±0.0032
8	0.0617±0.0124	0.1170±0.0096	0.1500±0.0063	0.7360±0.0044
9	0.0271±0.0100	0.0755±0.0095	0.1790±0.0080	0.6550±0.0057
10	0.0064±0.0058	0.0473±0.0089	0.1030±0.0075	0.5730±0.0069
11	0.0006±0.0020	0.0278±0.0080	0.0974±0.0084	0.5010±0.0081
12	0.0002±0.0013	0.0141±0.0065	0.0466±0.0068	0.4170±0.0091
13	0.0000±0.0000	0.0037±0.0038	0.0392±0.0071	0.3300±0.0098
14	0.0000±0.0000	0.0013±0.0025	0.0275±0.0067	0.2820±0.0105
15	0.0000±0.0000	0.0010±0.0024	0.0198±0.0063	0.2140±0.0106
16	0.0000±0.0000	0.0002±0.0012	0.0129±0.0056	0.1670±0.0106
17	0.0000±0.0000	0.0000±0.0000	0.0086±0.0050	0.1260±0.0103
18	0.0000±0.0000	0.0000±0.0000	0.0066±0.0048	0.0978±0.0101
19	0.0000±0.0000	0.0000±0.0000	0.0038±0.0040	0.0695±0.0093
20	0.0000±0.0000	0.0000±0.0000	0.0036±0.0042	0.0467±0.0084
21	0.0000±0.0000	0.0000±0.0000	0.0022±0.0035	0.0891±0.0122
22	0.0000±0.0000	0.0000±0.0000	0.0010±0.0025	0.0602±0.0109
23	0.0000±0.0000	0.0000±0.0000	0.0001±0.0009	0.0408±0.0097
24	0.0000±0.0000	0.0000±0.0000	0.0000±0.0000	0.0259±0.0083
25	0.0000±0.0000	0.0000±0.0000	0.0000±0.0000	0.0169±0.0072
26	0.0000±0.0000	0.0000±0.0000	0.0000±0.0000	0.0114±0.0062
27	0.0000±0.0000	0.0000±0.0000	0.0000±0.0000	0.0205±0.0088
28	0.0000±0.0000	0.0000±0.0000	0.0000±0.0000	0.0113±0.0070
29	0.0000±0.0000	0.0000±0.0000	0.0000±0.0000	0.0061±0.0054
30	0.0000±0.0000	0.0000±0.0000	0.0000±0.0000	0.0024±0.0036

Table 5: Underdensity Probability Function $U(r)$ (using density threshold $\delta\rho/\rho = -0.8$) measured for volume-limited samples of the NGP region with absolute magnitude limits $M_{\text{lim}} - 5\log h = -18, -19, -20$ and -21 .

$r \ (h^{-1}\text{Mpc})$	-18	-19	-20	-21
1	0.9530 ± 0.0004	0.9760 ± 0.0002	0.9930 ± 0.0001	0.9990 ± 0.0000
2	0.7790 ± 0.0022	0.8620 ± 0.0011	0.9520 ± 0.0004	0.9950 ± 0.0001
3	0.5470 ± 0.0050	0.6840 ± 0.0027	0.8680 ± 0.0011	0.9790 ± 0.0003
4	0.3590 ± 0.0074	0.4880 ± 0.0044	0.7360 ± 0.0023	0.9580 ± 0.0006
5	0.3110 ± 0.0099	0.3220 ± 0.0058	0.5890 ± 0.0036	0.9210 ± 0.0011
6	0.2890 ± 0.0128	0.3120 ± 0.0076	0.4430 ± 0.0048	0.8680 ± 0.0019
7	0.2160 ± 0.0146	0.2550 ± 0.0090	0.3160 ± 0.0056	0.8080 ± 0.0027
8	0.1610 ± 0.0159	0.2480 ± 0.0109	0.3570 ± 0.0071	0.7290 ± 0.0037
9	0.1370 ± 0.0178	0.1720 ± 0.0113	0.2460 ± 0.0076	0.6420 ± 0.0048
10	0.1030 ± 0.0184	0.1440 ± 0.0123	0.2340 ± 0.0087	0.5600 ± 0.0058
11	0.0813 ± 0.0191	0.1180 ± 0.0131	0.1500 ± 0.0085	0.4720 ± 0.0068
12	0.0631 ± 0.0194	0.0897 ± 0.0132	0.1270 ± 0.0090	0.3800 ± 0.0075
13	0.0440 ± 0.0184	0.0701 ± 0.0133	0.0964 ± 0.0090	0.3000 ± 0.0080
14	0.0288 ± 0.0168	0.0495 ± 0.0126	0.0756 ± 0.0090	0.2340 ± 0.0083
15	0.0099 ± 0.0110	0.0317 ± 0.0113	0.0519 ± 0.0084	0.1690 ± 0.0081
16	0.0026 ± 0.0062	0.0209 ± 0.0102	0.0443 ± 0.0086	0.1280 ± 0.0080
17	0.0009 ± 0.0040	0.0119 ± 0.0085	0.0334 ± 0.0082	0.0856 ± 0.0073
18	0.0001 ± 0.0015	0.0068 ± 0.0070	0.0261 ± 0.0079	0.1640 ± 0.0105
19	0.0000 ± 0.0000	0.0043 ± 0.0060	0.0195 ± 0.0075	0.1210 ± 0.0101
20	0.0000 ± 0.0000	0.0010 ± 0.0031	0.0129 ± 0.0066	0.0755 ± 0.0088
21	0.0000 ± 0.0000	0.0005 ± 0.0024	0.0106 ± 0.0064	0.0507 ± 0.0079
22	0.0000 ± 0.0000	0.0000 ± 0.0000	0.0054 ± 0.0049	0.0287 ± 0.0064
23	0.0000 ± 0.0000	0.0000 ± 0.0000	0.0032 ± 0.0041	0.0459 ± 0.0086
24	0.0000 ± 0.0000	0.0000 ± 0.0000	0.0027 ± 0.0040	0.0271 ± 0.0071
25	0.0000 ± 0.0000	0.0000 ± 0.0000	0.0012 ± 0.0028	0.0151 ± 0.0057
26	0.0000 ± 0.0000	0.0000 ± 0.0000	0.0002 ± 0.0012	0.0159 ± 0.0062
27	0.0000 ± 0.0000	0.0000 ± 0.0000	0.0000 ± 0.0000	0.0102 ± 0.0052
28	0.0000 ± 0.0000	0.0000 ± 0.0000	0.0000 ± 0.0000	0.0125 ± 0.0061
29	0.0000 ± 0.0000	0.0000 ± 0.0000	0.0000 ± 0.0000	0.0063 ± 0.0046
30	0.0000 ± 0.0000	0.0000 ± 0.0000	0.0000 ± 0.0000	0.0057 ± 0.0046

Table 6: Underdensity Probability Function $U(r)$ (using density threshold $\delta\rho/\rho = -0.8$) measured for volume-limited samples of the SGP region with absolute magnitude limits $M_{\text{lim}} - 5\log h = -18, -19, -20$ and -21 .

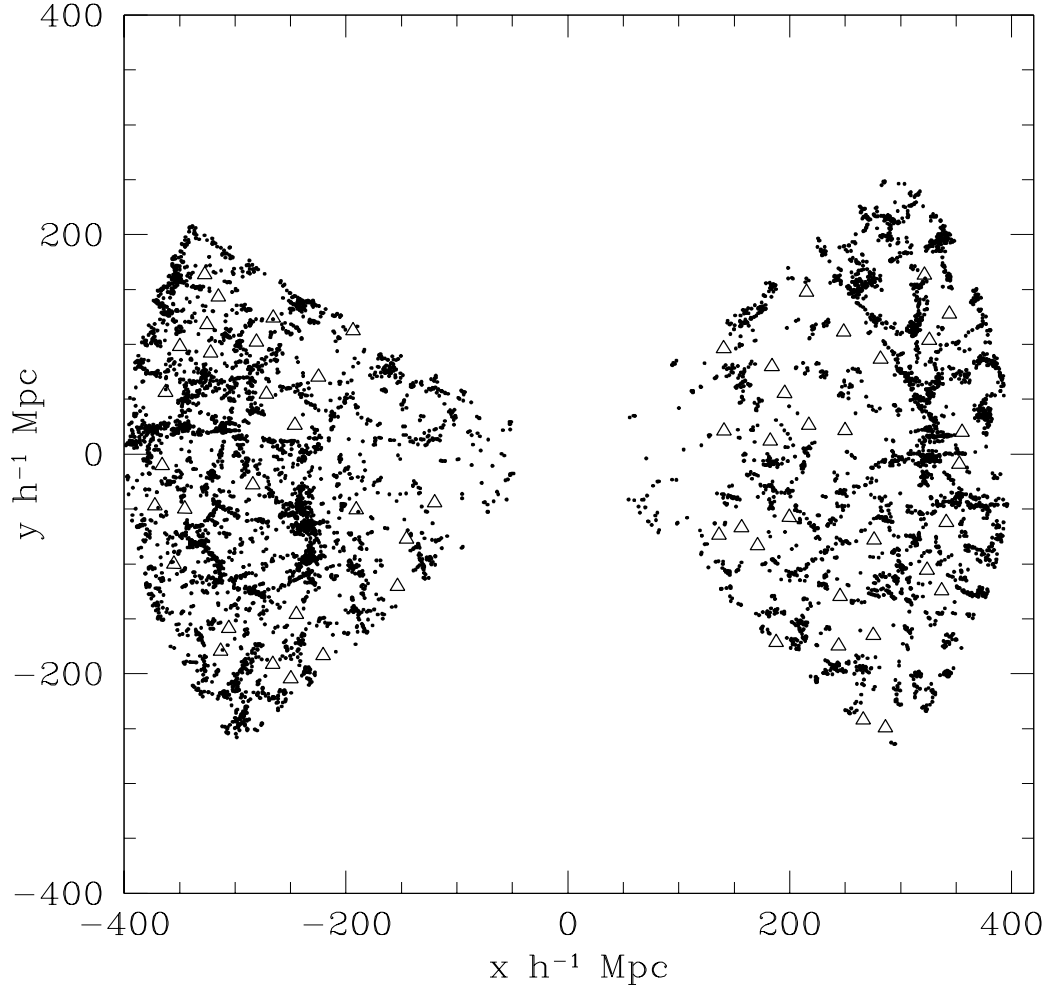


Fig. 1.— Voids in the NGP and SGP. Here we show an example of the distribution of wall galaxies (filled points) and the centers of voids (open triangles) in thin (1°) slices of the NGP and SGP.

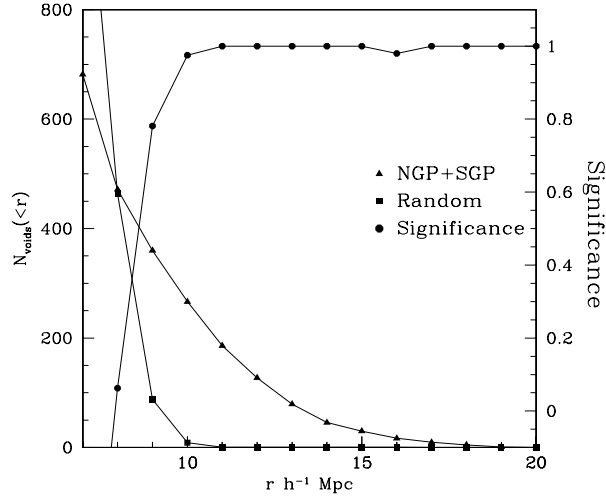


Fig. 2.— Statistical significance of voids. Triangles show the cumulative distribution of voids in the NGP and SGP, extended below a maximal sphere radius of $10h^{-1}\text{Mpc}$ for this purpose only. Squares show the cumulative distribution of voids in random samples, averaged over 10 realizations. Circles show the void significance at each scale. All voids larger than $10h^{-1}\text{Mpc}$ are significant at the 90% level. On smaller scales the significance drops rapidly.

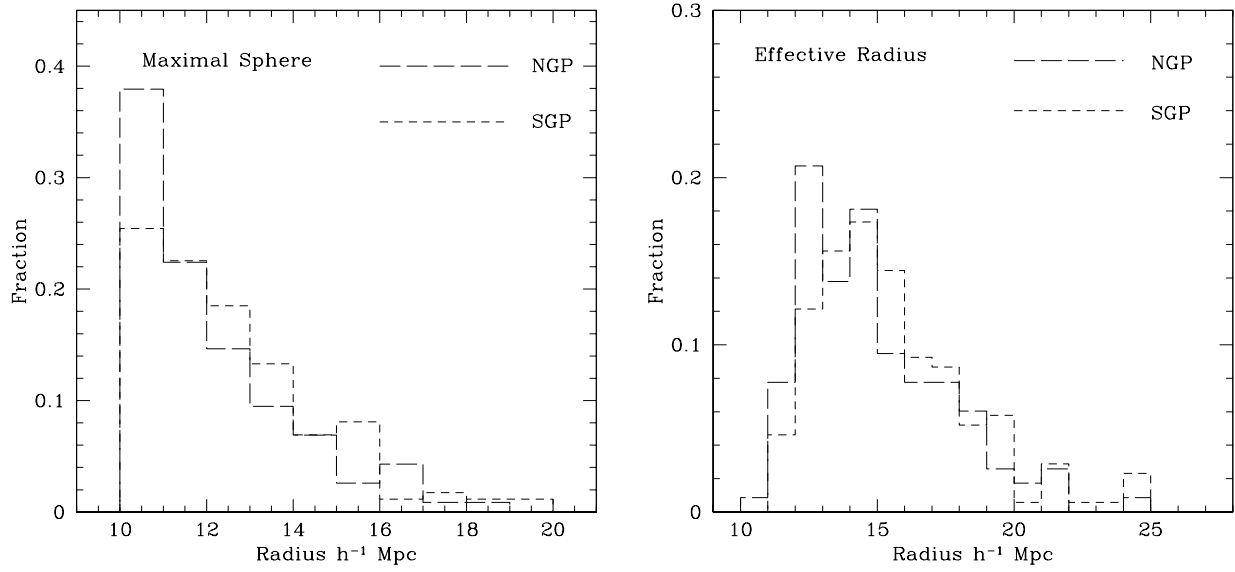


Fig. 3.— Distribution of maximal sphere sizes and effective radii for the voids in the NGP (long dashed line) and the SGP (short dashed line). The average maximal sphere size is $12.09 \pm 1.85h^{-1}\text{Mpc}$ for the NGP and $12.52 \pm 1.99h^{-1}\text{Mpc}$ for the SGP and the average effective void size is $14.89 \pm 2.65h^{-1}\text{Mpc}$ for the NGP and $15.61 \pm 2.84h^{-1}\text{Mpc}$ for the SGP.

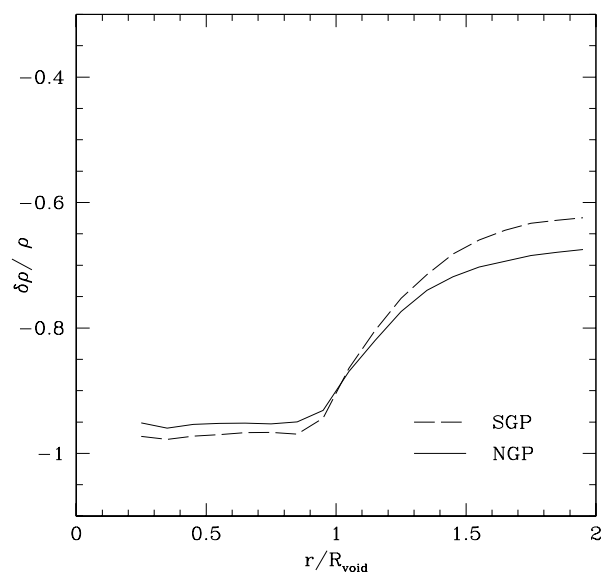


Fig. 4.— Radial density profile of voids. Within the void radius ($r/R_{\text{void}} < 1$), the voids are very empty, with density contrast ($\delta\rho/\rho < -0.9$). Just beyond the maximal sphere radii the density of the voids rises rapidly. However, even at twice the void radius, the density remains lower than average.

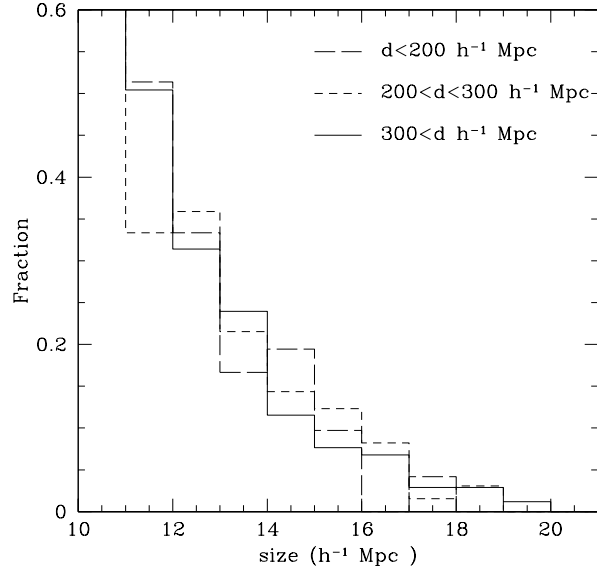


Fig. 5.— Test for evolution of void sizes. Lines show the fraction of voids as a function of the maximal sphere radius split into three groups by comoving distance: $< 200h^{-1}\text{Mpc}$ (long-dash), $200 - 300h^{-1}\text{Mpc}$ (short dash) and $> 300h^{-1}\text{Mpc}$ (solid). There is little difference in the histograms, hence no indication of evolution in the sizes of voids over the range of redshift covered by the 2dFGRS.

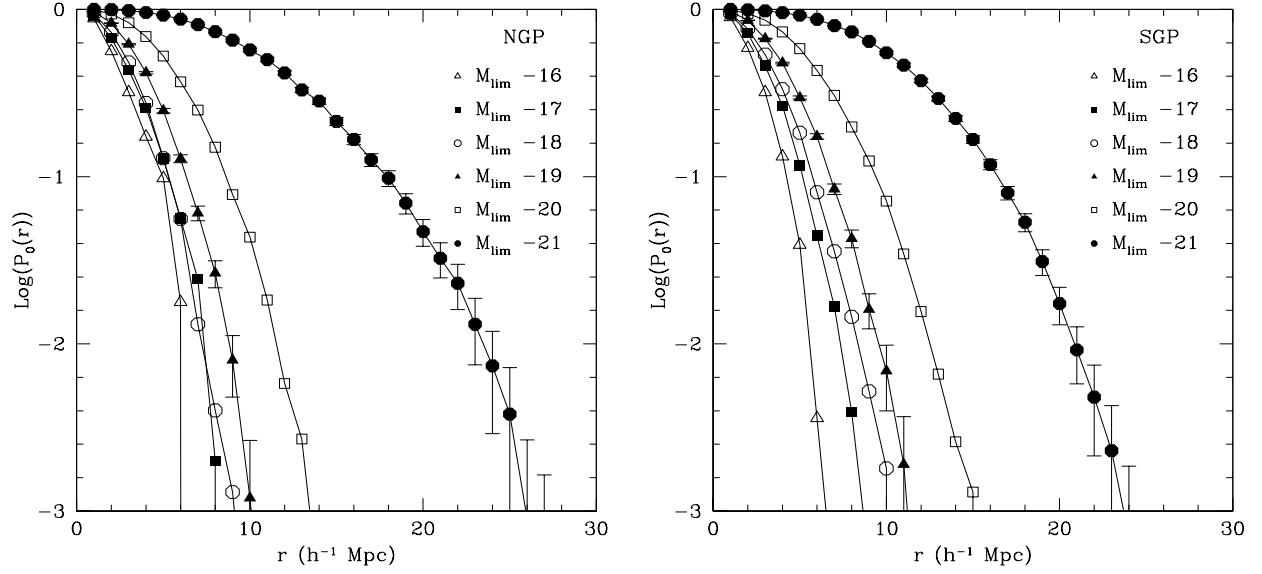


Fig. 6.— Void Probability Functions (VPF) for volume-limited samples extracted from the NGP (left hand plot) and SGP (right hand plot) regions of the 2dFGRS. The details of each of the samples are given in Table 2. Errorbars on the $M_{\text{lim}} = -19$ and -21 samples are the 1σ variation due to the finite number of independent volumes in the 2dFGRS.

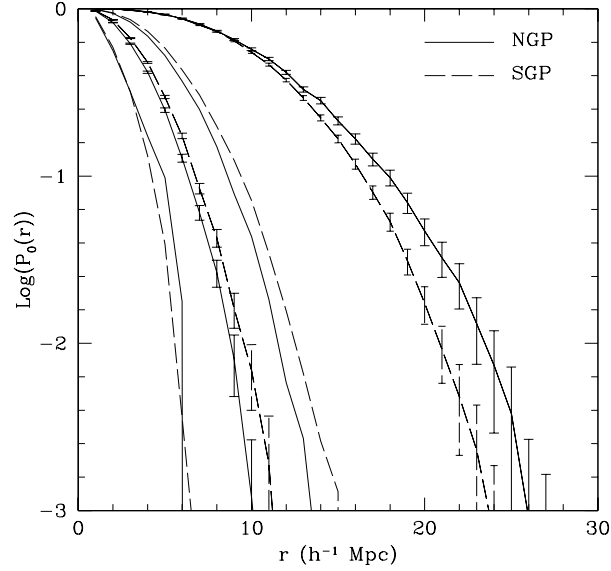


Fig. 7.— Comparison of VPF’s measured for the NGP (solid lines) and SGP (dashed lines) of 4 of the 6 samples shown above: $M_{\text{lim}} = -16, -19, -20$ and -21 ($z_{\text{max}}=0.039, 0.126, 0.182$ and 0.270). We see that locally (for all but the brightest sample), there is a higher probability of finding voids in the SGP (the lines are shifted to the right). This is consistent with the results of `voidfinder`; the SGP is emptier than the NGP. In the brightest sample, voids are more likely to be detected in the NGP.

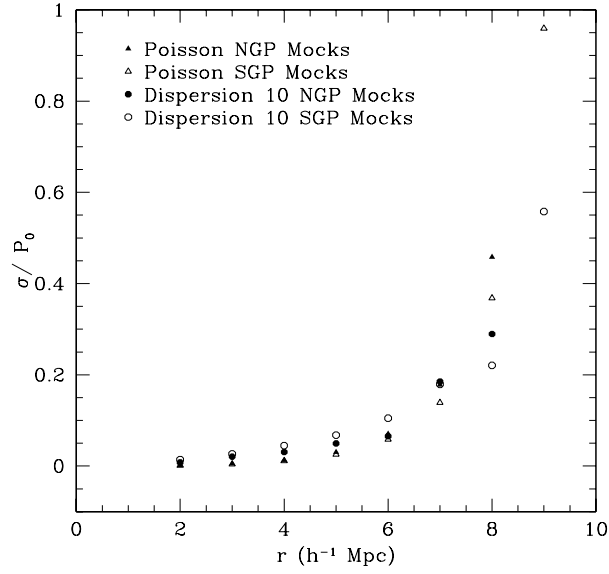


Fig. 8.— Comparison of methods for estimating uncertainties in the VPF, using the Poisson type errors of equation 6 (triangles) and the dispersion over 10 mock catalogs (circles). We show the results for the NGP (filled symbols) and the SGP (open symbols). The two methods give similar errors, although the Poisson errors are smaller on small scales and larger on large scales, as compared to the errors from the mock catalogs.

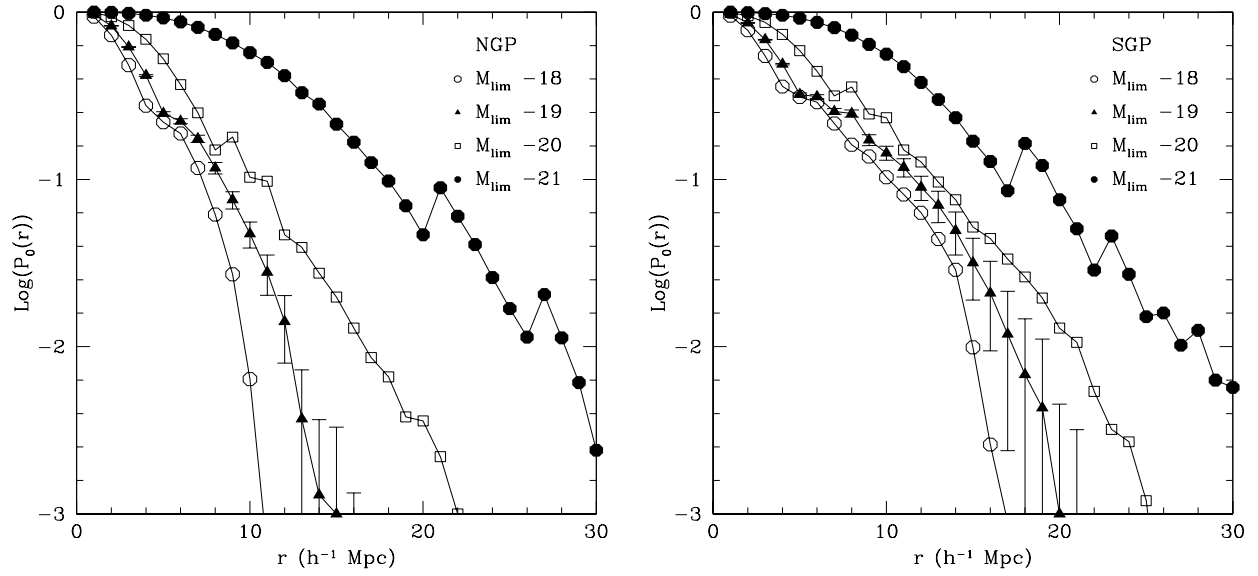


Fig. 9.— Underdensity Probability Function at density threshold $\delta\rho/\rho = -0.8$ for volume-limited samples extracted from the NGP (left hand plot) and SGP (right hand plot). Details of each of the samples are given in Table 2. For clarity, error bars are shown on the -19 samples only and are the 1σ variation due to the finite number of independent volumes in the 2dFGRS.

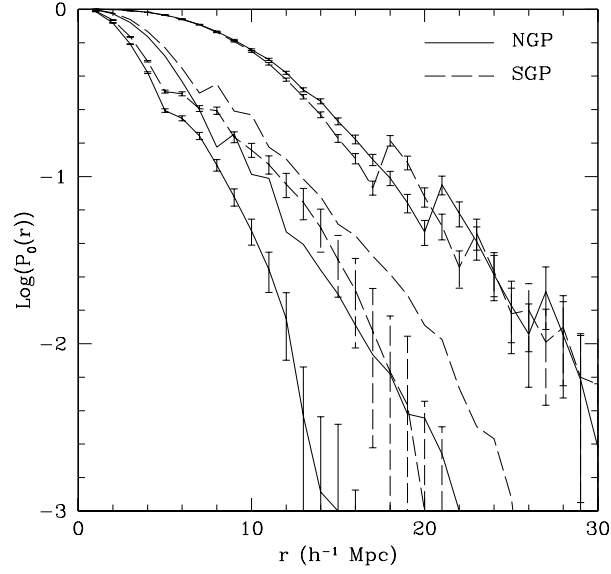


Fig. 10.— Comparison of the UPF's of the NGP (solid lines) and SGP (dashed lines) the samples with $M_{\text{lim}} = -19, -20$ and -21 ($z_{\text{max}}=0.126, 0.182$ and 0.270). Again, we see that locally, there is a higher probability of finding underdense regions in the SGP, the lines are shifted to the right. In this case though, there is good agreement between the brightest samples.

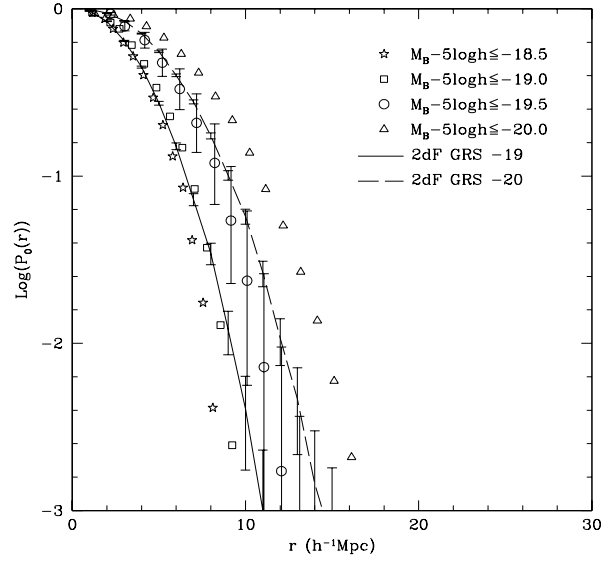


Fig. 11.— Comparison of the 2dFGRS VPF’s with earlier results from the CfA2 (Vogeley et al. 1994). Symbols show the VPF’s from CfA2 and lines show results from the 2dFGRS. Errorbars are shown on the -19.5 CfA2 sample and on the 2dFGRS samples. Taking into account a zeropoint shift of roughly $m_Z = b_j + 0.5$, we note that the -18.5 CfA2 sample and -19.0 2dFGRS samples agree within the errors (which are strongly correlated), as do the -19.5 CfA2 and -20.0 2dFGRS samples.

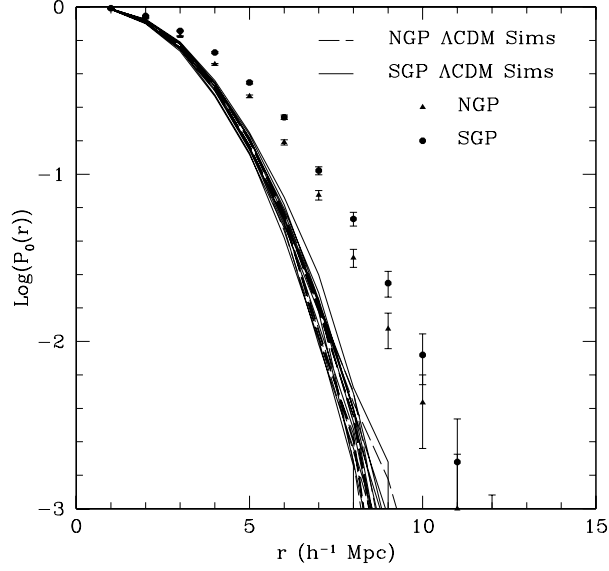


Fig. 12.— Comparison of the VPF of the 2dFGRS with the VPF of mock catalogs drawn from a dark matter only Λ CDM simulation, the *Hubble Volume*. The dark matter only mock catalogs contain too much substructure and fail to match the VPF’s of the data, as seen in Benson et al. (2003).

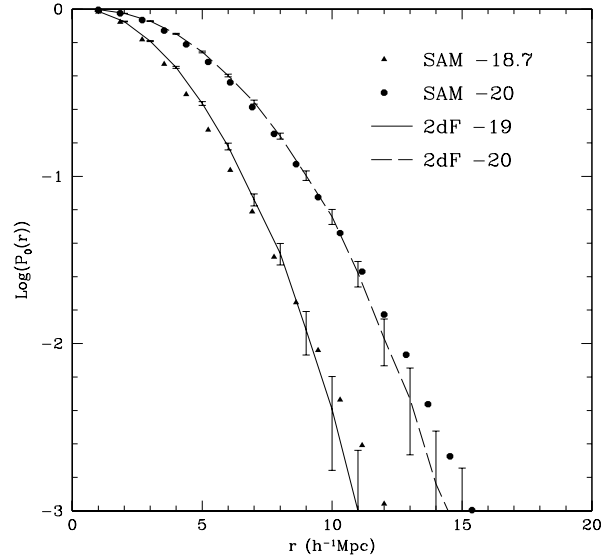


Fig. 13.— Comparison of the 2dFGRS VPF’s and those from the mock semi-analytic galaxy catalogs of Benson et al. (2003). There is excellent agreement between the theory and the data.